Anomalous Diffusion in Associative Networks of High Sticker-Density Polymers

Irina Mahmad Rasid,[†] Niels Holten-Andersen[,†] and Bradley D. Olsen*[,‡]*

[†] Department of Materials Science and Engineering, Massachusetts Institute of Technology, 77 Massachusetts Avenue, Cambridge, Massachusetts 02139, United States

[‡] Department of Chemical Engineering, Massachusetts Institute of Technology, 77 Massachusetts Avenue, Cambridge, Massachusetts 02139, United States

ABSTRACT: Recent experiments on self-diffusion in associative networks have shown superdiffusive scaling hypothesized to originate from molecular diffusive mechanisms which include walking and hopping of the polymer chains. Since hopping requires the release of all the stickers on the chain, it is expected that as the sticker density is increased, the walking mode will become dominant such that eventually only Fickian scaling will be observed for polymers with sticker-densities above a critical value. In this work, a set of copolymers of *N,N*-dimethyl acrylamide and pendant histidine groups with sticker densities ranging from 4 to 15 stickers per chain was synthesized using RAFT polymerization. The self-diffusion of the polymer chains in the gels in the unentangled regime was then studied using forced Rayleigh scattering (FRS). For the range of length scales measured, superdiffusive scaling was observed across the entire range of sticker densities. This suggest that molecular hopping is an important mechanism for diffusion,

even for the polymer with the highest sticker density. Further analysis shows that hopping of the high-sticker density polymer is promoted by the presence of a significant fraction of intrachain bonds, the entropic penalty associated with binding to the network, and the distribution of sticker densities inherent to copolymers synthesized through RAFT polymerization.

INTRODUCTION

Associative networks are a versatile class of soft materials that has been employed for various applications such as wearable devices[1-2], soft electronics[3-4], self-healing coatings[5-6], injectable hydrogels[7-8], and enhanced oil recovery (EOR) fluids[9-10]. These networks show diverse viscoelastic responses based on various design factors including sticker valency[11], chain architecture[12-13] and sticker density[12, 14]. Beyond mechanical properties, diffusion through associative networks is also important in both natural and synthetic materials. For example, transport of target molecules into the nucleus of cells is achieved through weak binding associations with proteins in the nuclear pore complex.[15] It has been shown that the presence of multiple associative sites on the target molecules can enhance diffusion by increasing the interaction with the matrix of the nuclear pore complex. [15-16] In synthetic systems, the self-diffusion of polymer chains dictates time scales for network recovery, which is key for the design of self-healing[17] and injectable hydrogels[18]. Elucidating the factors affecting self-diffusion in associative networks will aid in our ability to design new engineering materials and improve our understanding of the properties of natural materials.

The viscoelastic and transport properties of unentangled associative networks are determined by the dynamics of bond dissociation and reassociation. While viscoelasticity in these networks has been studied extensively, self-diffusion has been less explored. For self-diffusion, Baxandall

proposed a mean-field approach where the diffusivity of associative chains in a network of itself would resemble Rouse motion of non-associative chains but reduced by a factor of the characteristic time for reorganization of a crosslink and the sticker density S (defined as number of stickers per chain).[19] Rubinstein and Semenov then proposed the sticky Rouse model where they studied several concentration regimes, and their model showed that the characteristic time is expected to have a concentration dependence due to the conversion of intrachain to interchain bonds with increasing concentration.[20] While these models provide a framework to predict the effects of sticker density and concentration on polymer chain dynamics[20], they are not able to fully capture the diffusive behavior of the polymer chains. Tang *et al.* showed that at length scales of several times the radius of gyration R_g, phenomenological superdiffusive scaling was observed in several associative networks with $S = 4$ [21-22] prior to transitioning into the Fickian regime, an effect that is not predicted by mean-field models. The empirical two-state model developed by Tang *et al.* was able to quantitatively capture the superdiffusive scaling but was unable to provide molecular-level insights into its origin.[21] Based upon scaling arguments and molecular modeling, [23] Ramirez *et al.* later attributed the observation of superdiffusive scaling in tetra-PEG gels[22] to the existence of two diffusive modes, walking and hopping. The hopping mode corresponds to a polymer chain releasing all its stickers to diffuse a distance of several times R_g. For chains with high sticker densities ($\sim S > 5$), the probability of a chain releasing all its stickers to undergo hopping is greatly diminished, and the diffusion profile is expected to show only Fickian diffusion, as predicted by the mean-field approach. Recently, Rapp *et al.* developed a thermodynamic model that was able to capture the effect of increasing sticker density on diffusion in a protein gel, as measured using fluorescence recovery after photobleaching (FRAP). Their work showed that hopping could be an important mode for diffusion, even for chains with up to $S = 5$.[24] Therefore,

further experimental studies are needed to determine the regimes where the diffusive behavior seen in the molecular model (hopping and walking) persists and the transition point to where the mean-field approach is sufficient to capture the self-diffusion of associative polymers in the unentangled regime.

In this work, the self-diffusion of a set of hydrogels with varying sticker densities was measured using FRS. The hydrogels were prepared with linear copolymers of *N,N*-dimethyl-acrylamide and a histidine-functionalized monomer such that transient metal-coordinate crosslinks are formed upon addition of Ni^{2+} ions and adjustment of the pH to 7 (Figure 1). In the presence of the buffer, the Debye length for the Ni^{2+} ions are significantly smaller than the estimated spacing between stickers such that long-range electrostatic interactions are not expected to contribute to the crosslinking behavior (see supplementary information for calculations). The copolymers were prepared by RAFT polymerization, allowing for low molecular weight dispersity to be achieved. The monomer feed ratio was varied to synthesize polymers with sticker densities up to 15 stickers per chain. Fits to the two-state model provide a method to compare the diffusion profiles and suggest that hopping remains an important mode of diffusion even for the hydrogel prepared with the polymer of the highest sticker density.

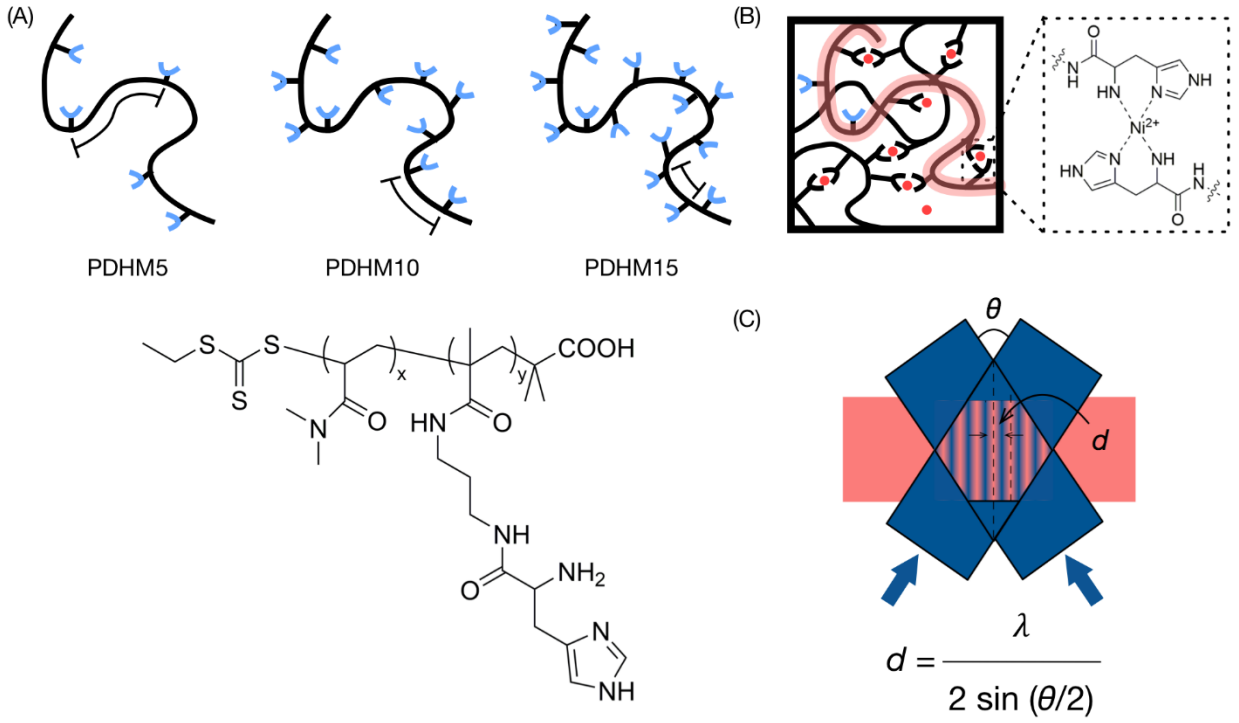

Figure 1. (A) Linear copolymers of *N*,*N*-dimethyl-acrylamide and a histidine-functionalized monomer were synthesized by varying the monomer feed ratio to achieve average sticker densities, *S*, of 5, 10 and 15 stickers per chain. The degree of polymerization ($N = x + y$) in all cases is N~250 such that the average sticker spacing $l = N/S$ for each polymer decreases with increasing sticker density. (B) Upon addition of Ni^{2+} ions, a purely associative network is formed with Ni-histidine bis-complexes as the primary crosslinks (proposed structure is shown on the right). Chain highlighted in red schematically represents a polymer chain labelled with a single fluorescein molecule. (C) Forced Rayleigh scattering forms one-dimensional concentration grating in the gel within the region of constructive interference where the photochromic dyes are irreversibly isomerized.

EXPERIMENTAL SECTION

The polymers in this work were synthesized through RAFT polymerization and the polymer synthesis and characterization are described in section C of the supplementary information (page 6). The properties of the polymers are summarized in Table 1.

Table 1. The calculated mole percent histidine (from ^{1}H NMR), average number of stickers per chain, *S,* average degree of polymerization, *N,* average spacing between stickers, *l*, chain overlap, $\phi_{overlap}$, entanglement, ϕ_e, and overlap of strand between stickers, ϕ_s, concentration for each polymer.

Polymer	Mol% HisMA	*S*	*N*	*l*	$\phi_{overlap}$ (w/v)	ϕ_e (w/v)	ϕ_s (w/v)
PDHM4FS	2.09	3.93	189	48	3.5%	41%	5.9%
PDHM5	2.09	4.98	238	48	3.1%	36%	5.9%
PDHM6FS	1.96	6.44	330	51	2.6%	29%	5.6%
PDHM10	3.74	9.58	256	27	3.0%	34%	9.4%
PDHM15	5.50	15.3	277	18	2.8%	32%	13%

Gel Preparation. The gels of the PDMA polymers with pendant histidine groups were prepared following previously published procedures.[25] The polymers were first dissolved in a Bis-Tris buffer (100 mM, pH 7.0), to which the appropriate amount of a stock solution containing 200 mM $NiCl_2$ and 100 mM Bis-Tris was added. The mixture was vortexed for 15 s. Once mixed, the appropriate amount of a stock solution of 1 M NaOH with 100 mM Bis-Tris buffer was then added to adjust the pH to 7.0. The gels were then mixed with a micro spatula until a macroscopically homogenous gel was obtained. Finally, the gels were centrifuged at 21,100 g to remove air bubbles

introduced during mixing. The amount of $NiCl_2$ stock solution required was determined by ^1H NMR (Figure S1), while the amount of NaOH stock solution required was determined by titration experiments in dilute solution (see Section C in supplementary information).

Forced Rayleigh Scattering. For self-diffusion measurements, 20 μM of the fluorescein-labelled polymers (P2) was added to the dissolved P1 polymer solution before the addition of $NiCl_2$ stock solution during the gel preparation. All samples were sealed between two quartz disks (17 mm in diameter) separated by a 0.2 mm thick Teflon spacer and were left overnight at room temperature to eliminate shear history from loading. Samples were equilibrated at the desired temperature for 1 h before further experiments were performed. Samples that were not equilibrated gave decay curves that exhibited additional relaxation processes that were not reproducible when different positions on the sample were tested (Figure S2), and this was used to determine the minimum time required for equilibration. The self-diffusion measurements were performed using forced Rayleigh scattering (FRS), as previously described. [21, 26-27] Briefly, a 100 mW continuous wave laser with λ = 488 nm was split into two beams, which were individually refocused and crossed on the sample at an angle θ. This generated a holographic grating of characteristic spacing d that is defined by the following equation

$$d = \frac{\lambda}{2\sin(\theta/2)} \quad (1)$$

On exposure of the sample for 100-500 ms, the photochromic fluorescein dye conjugated to the tracer molecules was irreversibly isomerized in the areas of constructive interference, producing an amplitude grating of dye concentration. Diffusion of the dye results in a sinusoidal concentration profile by diffusion, which was monitored by diffraction of a single reading beam at the same wavelength. The intensity of the reading beam was attenuated by 10^{-4} so that it was low enough to ensure the change of the profile was only due to diffusion. The time constant, τ, can

be extracted from fitting either a single stretched exponential function or a sum of two exponential functions to the signal:

$$I = A\exp^2\left[-\left(\frac{t}{\tau}\right)^{\beta}\right] + B \tag{2}$$

$$I = A_1\exp^2\left[-\left(\frac{t}{\tau_1}\right)^{\beta_1}\right] + A_2\exp^2\left[-\left(\frac{t}{\tau_2}\right)^{\beta_2}\right] + B \tag{3}$$

where I is the intensity, β is the stretched exponent ranging from 0 to 1, and B is the incoherent background. The average decay time constant was calculated as the first moment of the stretched exponential:

$$\langle\tau\rangle = \frac{\tau_{KWW}}{\beta}\Gamma\left(\frac{1}{\beta}\right) \tag{4}$$

where Γ is the gamma function. Example fits are shown in Figure 2.

RESULTS AND DISCUSSION

Evidence for two relaxation modes. The FRS signal obtained from the gels investigated in this work can be fit to a single exponential function or a sum of two exponential functions. The presence of two relaxation modes in the regime where superdiffusive scaling is observed was predicted by Ramirez *et al.*'s molecular model[23] and the two-state model[21]. In previous work with FRS measurements of self-diffusion of unentangled associative networks [21-22], only a single exponential decay was observed, presumably because the fast relaxation mode was not experimentally accessible. For the gels investigated in this work, faster decays (~100 s) resulted in curves that can be fit well with a single exponential function, with longer decays (~3000 s)

showing greater deviations. In Figure 2, the results of fitting the two functions for a relatively long decay are shown for comparison. The fit the to a single stretched exponential provides a reasonable fit to the measured signal (Figure 2 A(i)). However, it is apparent from the plot of the residual that the function does not fully capture the decay (Figure 2 A(ii)) and in this case, the function with two exponential terms gives an improved fit (Figure 2 B(i and ii)).

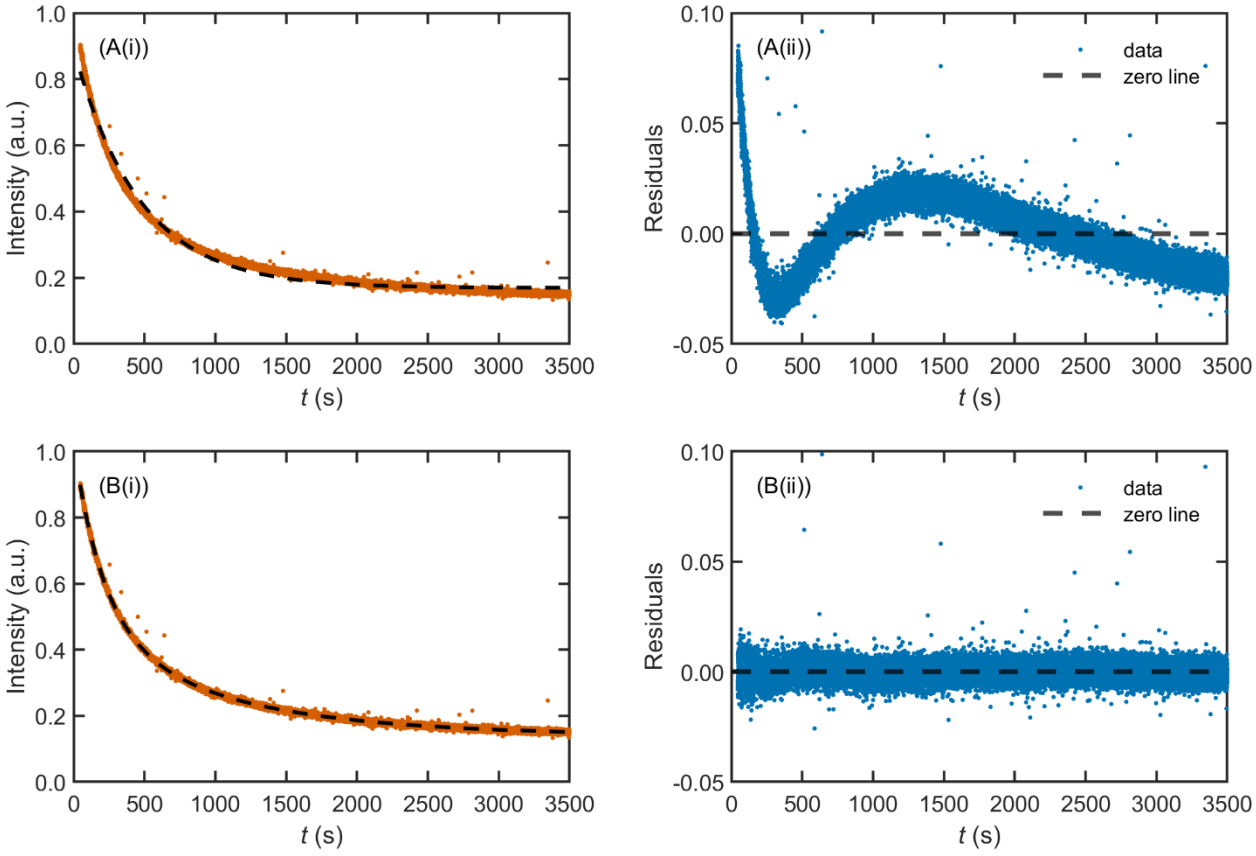

Figure 2. An example showing the decay in intensity over time (orange dots). (A) (i and ii) The fit to a single stretched exponential function (eq 2) gave a reasonable fit, but the residuals indicate a contribution from a second exponential term. (B) (i and ii) The fit to a sum of two stretched exponential function (eq 3) resulted in smaller residuals that do not show a time-dependence. Data acquired for PDHM15 25% (w/v) at $\theta = 2°$ ($d^2 = 195.5\ \mu m^2$) and temperature of 35 °C.

The decay signals for gels with PDHM5, PDHM10 and PDHM15 at 25% (w/v) were fit to both a single exponential function or a sum of two exponential functions (eq 2 and eq 3, respectively) and the average decay time constants $\langle\tau\rangle$, $\langle\tau_1\rangle$ and $\langle\tau_2\rangle$ were calculated using eq 4 (Figure 3(A-C)).

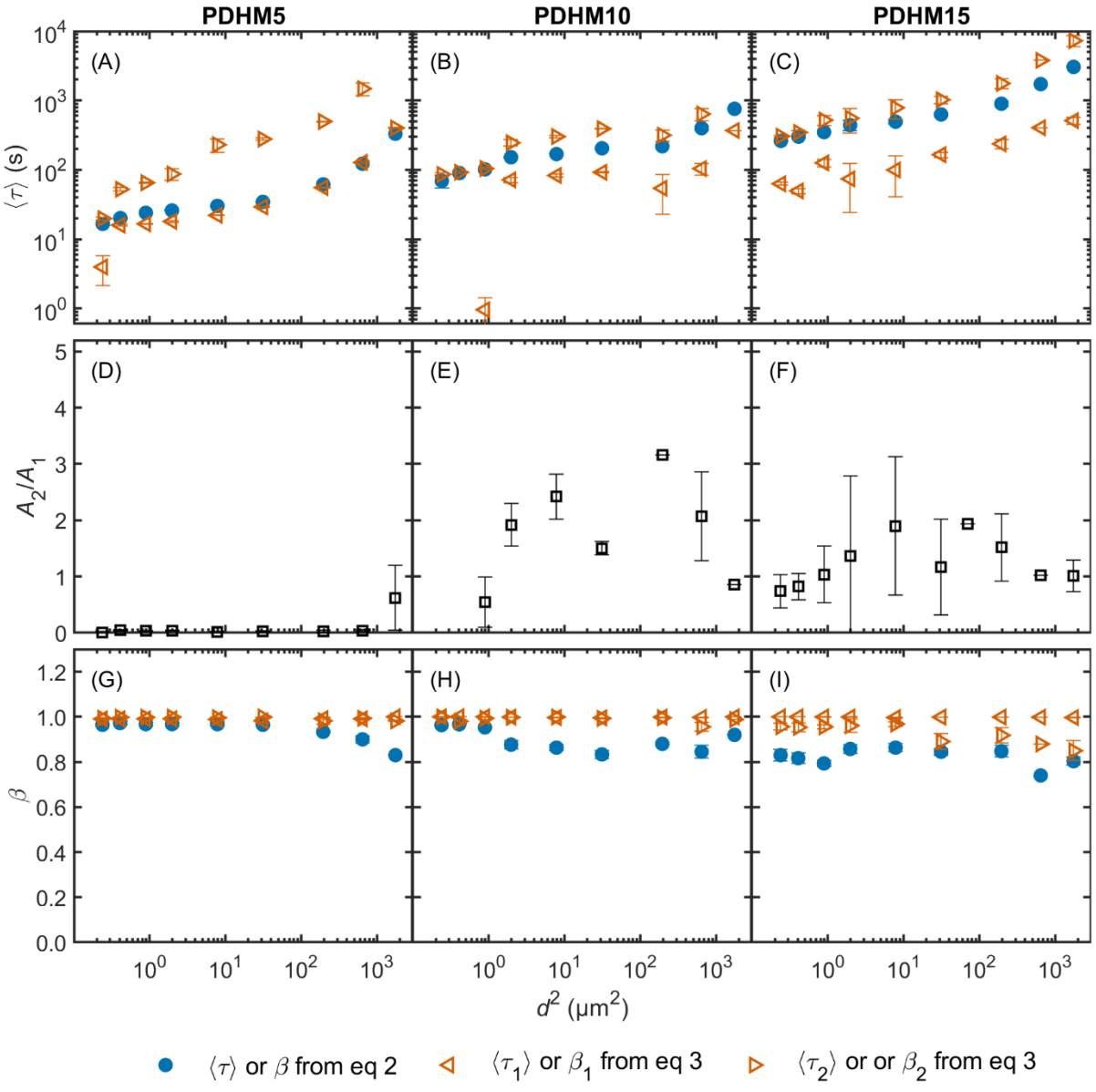

Figure 3. (A-C) The plot of $\langle\tau_1\rangle$ and $\langle\tau_2\rangle$ from the fits to eq 3, compared to $\langle\tau\rangle$ from the fit to eq 2, (D-F) A_2/A_1 from the fit to a sum of two exponential fits and (G-I) the β exponent from the single exponential fit, for PDHM5, PDHM10 and PDHM15 at 25% (w/v), respectively, as a function of

d^2, the square of the characteristic spacing in the holographic grating defined by eq (1. Error bars represent standard error of measurements performed in triplicate. Error bars for filled symbols are smaller than the symbols.

The relative contributions of $\langle\tau_1\rangle$ and $\langle\tau_2\rangle$ can be seen from the plot of A_2/A_1 where τ_2 corresponds to the longer time constant (Figure 3(D-F)). The value A_2/A_1 varies from ~0-3 as the decay times increase, as indicated by larger $\langle\tau\rangle, \langle\tau_1\rangle$ and $\langle\tau_2\rangle$ in Figure 3(A-C). With decreasing decay times, it becomes more difficult to obtain a reliable fit to the function with two exponential terms, as seen with the increased scatter for $\langle\tau_1\rangle$ and $\langle\tau_2\rangle$ for the PDHM10 gel. With the shortest decay times for PDHM5, $A_2/A_1 \sim 0$ for most range of d^2 and this is because the fast relaxation mode was insufficiently captured and $\langle\tau_2\rangle$ in this case has no significance. For fits to the single exponential function, less scatter is seen in the values of $\langle\tau\rangle$ because the fit is less sensitive to how much of the fast relaxation mode was captured in the raw data. The value of the β exponent from the single exponential fit is sensitive to the presence of multiple relaxation modes. As the decay times increased, the β exponent begins to decrease from values that are close to 1 to ~0.8 (Figure 3(G-I)). The β exponent can vary between 0 and 1, where $\beta = 1$ is expected for decays with a single relaxation mode and greater deviation from 1 implies an increasingly broad decay due to the presence of multiple modes of relaxation. The values of $\langle\tau\rangle$ from longer decays are an approximation that slightly underestimates the longest relaxation time $\langle\tau_2\rangle$ due to the effect of the shorter relaxation time (Figure 3(C)).

The plots comparing the results of the fits to the single exponential function to that of the two exponential functions for all the gel concentrations investigated are shown in the supporting information (Figure S3). Based on these results, it is apparent that the values of $\langle\tau\rangle$ from the fits to the single exponential function for the PDHM5 gels and the values of $\langle\tau_2\rangle$ for the PDHM15 gels

effectively capture the longest relaxation time of these gels. For the PDHM10 gels however, the fast relaxation times are insufficiently captured to enable reliable fits to eq 3, and this results in significant scatter seen in the $\langle\tau_2\rangle$ values. A comparison of the results of the analysis based on the single and sum of two exponential fits is included in the supplementary information and demonstrates that $\langle\tau\rangle$ is a reasonable approximation for the PDHM10 gels, and the reduced scatter in the single exponential fits lead to physically more relevant results. Therefore, in the following section, further analysis will be performed on the results of the fits to the single exponential function for the PDHM5 and PDHM10 gels, and the results of the fits to the sum of two exponential functions for the PDHM15 gels.

Anomalous Diffusion in High-Sticker Density Polymers. The self-diffusion measurement of the model associative network in the unentangled regime, with sticker densities ranging from 5 to 15 stickers (Figure 4) revealed that apparent superdiffusive scaling was observed at the smaller end of the experimental length scale range, prior to transitioning to a Fickian scaling, even for the polymer with the highest sticker density. The concentrations investigated range from 15% to 30% (w/v) which correspond to concentrations above the concentration for overlap of the strand between stickers, ϕ_s, based on the scaling arguments in the sticky Rouse model where $\phi_s \approx l^{-0.77}$ ($\phi_s \sim S^{0.77}$ for fixed N).[20] The estimated ϕ_s are $\phi_{s,PDHM5} \approx 5.9\%$, $\phi_{s,PDHM10} \approx 9.4\%$, and $\phi_{s,PDHM15} \approx 12.8\%$. The observation of superdiffusive scaling in these linear, side-linked polymers shows similarities to two previously investigated systems: hydrogels formed by linear proteins with four associating coiled-coil domains[21] and four-arm star-shaped polymers end-functionalized with terpyridine moieties that are complexed with Zn^{2+} in DMF [22]. In the gels presented here, the self-diffusion curves shift to longer times (seen as a shift upwards) with increasing concentration and stickers per chain. Note that the time scales shown in Figure 4 are

longer than the time scales reported for tracer diffusion measurement of a histidine molecule within gels formed with histidine-Ni^{2+} using FRS across the entire range of length scales, consistent with diffusion of the polymers requiring the dissociation of multiple bonds. [25]

Table 2. The concentration of gels investigated in this work in terms of ϕ/ϕ_s, where ϕ_s is the concentration for overlap of the strand between stickers.

ϕ (w/v)	15%	20%	25%	30%
Polymer	ϕ/ϕ_s			
PDHM5	-	3.4	4.2	5.1
PDHM10	1.6	2.1	2.7	-
PDHM15	1.2	1.6	2.0	-

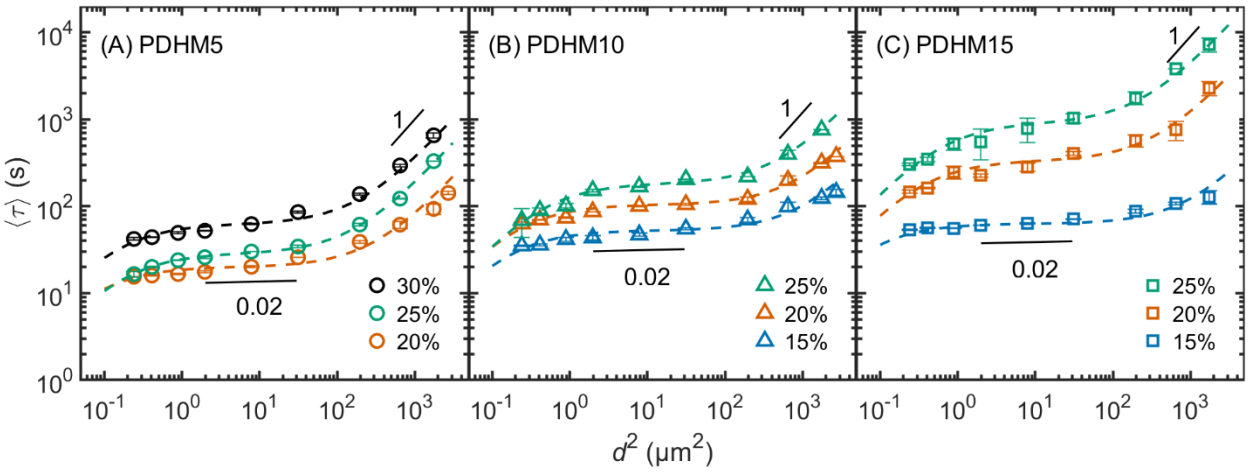

Figure 4. Plot of $\langle\tau\rangle$ vs d^2 for (A) PDHM5, (B) PDHM10 and (C) PDHM15 at 15%, 20%, 25% and 30% (w/v), measured at 35 °C. The molecular weight was held constant, while the sticker density was increased. The dashed lines are fits to the two-state model. Error bars represent standard error of measurements performed in triplicate.

The previously proposed two-state model for self-diffusion applied to the protein gel[21] and the four-arm star polymer[22] gel systems is also able to capture the self-diffusion over the entire range

of d^2 for the gels in this work. Briefly, the associative polymers in the network are hypothesized to exist in two states: a molecular state and an associated state. The two states are distinguished by their diffusivities, such that the diffusivity of the molecular state, D_{M}, is much larger than the diffusivity of the associated state, D_{A} (units: μm s^{-1}). The polymers interconvert between the two states with pseudo-first order kinetics, with interconversion rates k_{on} and k_{off} (units: s^{-1}):

$$\frac{\partial C_{\mathrm{M}}}{\partial t} = D_{\mathrm{M}} \frac{\partial^2 C_{\mathrm{M}}}{\partial x^2} - k_{\mathrm{on}} C_{\mathrm{M}} + k_{\mathrm{off}} C_{\mathrm{A}} \tag{5}$$

$$\frac{\partial C_{\mathrm{A}}}{\partial t} = D_{\mathrm{A}} \frac{\partial^2 C_{\mathrm{A}}}{\partial x^2} + k_{\mathrm{on}} C_{\mathrm{M}} - k_{\mathrm{off}} C_{\mathrm{A}} \tag{6}$$

where C_{M} and C_{A} are the concentrations of the molecular and associative species and the subscripts M and A denote the molecular and associative species, respectively. The equilibrium constant is defined as $K_{eq} = k_{\mathrm{on}}/k_{\mathrm{off}}$ and the ratio of the two diffusivities $\gamma = D_{\mathrm{A}}/D_{\mathrm{M}}$. The model is solved analytically using Fourier transform methods to obtain the relation $\langle\tau\rangle$ vs d^2.

Only three parameters can be independently determined without imposing a specified value of K_{eq} from nonlinear fits to the data as shown by Tang *et al.*[21], and these parameters are plotted in Figure 5 (A-C). The effective diffusivity in the large length-scale Fickian regime, $D_{\mathrm{M,eff}}$, is equivalent to $D_M/(1 + K_{eq})$ under the condition that $\gamma K_{eq} << 1$, when anomalous diffusion is observed. The molecular dissociation rate constant, k_{off}, should not be taken as a physical rate constant since the physical details of the two diffusive states are not specified in the model. Thus, this parameter may have an implicit concentration dependence, in addition to a temperature dependence. The final parameter, γK_{eq}, is the anomaly index and is equivalent to the ratio of the two diffusivities and rate constants, $D_A/D_M \cdot k_{on}/k_{off}$. Note that γK_{eq} is inversely proportional to the width of the superdiffusive regime.

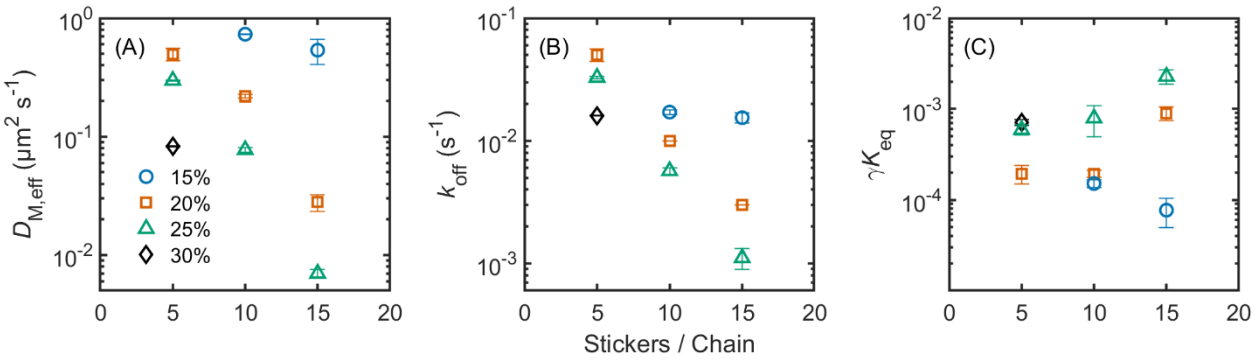

Figure 5. Effect of sticker density on (A) the effective diffusivity in the large-length-scale Fickian regime, $D_{M,eff}$ (B) the molecular dissociation rate, k_{off}, and (C) γK_{eq}. The parameters were obtained by fitting the analytical solution of the two-state model to the experimentally derived relation $\langle\tau\rangle$ vs d^2 for gels at various concentrations. Error bars represent 95% confidence intervals from fits to the two-state model.

Higher concentrations and sticker densities both lead to slower Fickian self-diffusion, as is apparent from the trends observed for $D_{\mathrm{M,eff}}$ in Figure 5(A). There is an order of magnitude difference in $D_{\mathrm{M,eff}}$ for the gels with 5 and 15 stickers per chain at 20 and 25% (w/v), consistent with the additional stickers along the backbone slowing down the rate of diffusion as more stickers must be released for the polymers to diffuse. Although the range of concentrations accessible for study is fairly narrow, scaling exponents can be roughly estimated in this regime using the three concentrations for each sticker density. The scaling of the Fickian diffusivity with concentration is $D_{\mathrm{M,eff}}{\sim}\phi^{-4\pm1}$, $D_{\mathrm{M,eff}}{\sim}\phi^{-5\pm1}$ and $D_{\mathrm{M,eff}}{\sim}\phi^{-12\pm1}$ for PDHM5, PDHM10 and PDHM15 respectively.

The sticky Rouse model predicts that for $\phi < \phi_s$, $D{\sim}\phi^{-5.19}$ and for $\phi > \phi_s$, $D{\sim}\phi^{-3}$ where ϕ_s is the concentration for overlap of strands between stickers.[20, 28] The model predicts that the concentration dependence is stronger for $\phi < \phi_s$ because in this regime increasing concentration results in the conversion of intrachain to interchain bonds. Above $\phi > \phi_s$, most stickers are already

in interchain bonds and thus a weaker decrease in D is seen from the increased density of crosslinks in a given volume. While the concentrations investigated in this work lie in the range of 1.2 – 5 ϕ_s (**Table 2**), the strong dependence of $D_{\mathrm{M,eff}}$ with ϕ is consistent with the regime where $\phi < \phi_s$. This suggests that the conversion of intrachain to interchain bonds is still occurring in these gels. Additionally, the stronger dependence of diffusivity on concentration shown by PDHM15 is due to the fact that $\phi_s \sim S^{0.77}$. As a result, for a given concentration of the gel, ϕ lies higher above ϕ_s for PDHM5 compared to PDHM15 such that a larger fraction of the stickers is still in intrachain bonds for PDHM15.

For length scales smaller than the regime where Fickian scaling is observed, superdiffusive scaling was observed for all the conditions investigated. Ramirez *et al.* developed a molecular model[23] which can capture the features observed here despite the fact that Ramirez *et al.* modeled star polymers and the polymers here are linear. In the model, molecular hopping and walking are the modes for diffusion for length scales greater than R_g, with superdiffusive scaling at intermediate length scales, which transitions into a Fickian regime at larger length scales. The effective diffusivity in their model is given by the sum of the walking and hopping diffusivities

$$D_{\mathrm{eff}} = D_{\mathrm{walk}} + D_{\mathrm{hop}} = \sum_{j=2}^{N_A} p_j k_D \frac{\langle R^2 \rangle}{j-1} + \frac{p_0}{N_A} \tag{7}$$

where N_A is the number of arms, or equivalently number of stickers for telechelic polymers, k_D is the kinetic constant of detachment and p_j is the probability that a molecule has j stickers attached to the network. While the general predictions of the molecular model are expected to apply to other chain architectures, the exact form of the model will be different for linear polymers. Thus, the model will not be used for fitting the data reported in this work but will instead be used as a

framework to guide the interpretation of the two-state model parameters. This approach enables further analysis of the results with regards to the molecular origin of the superdiffusive scaling.

While the predictions of the molecular model show good qualitative agreement with the general shape of the plots of $\langle\tau\rangle$ vs d^2 in Figure 4 (A-C), the values of k_{off} from the two-state model shown in Figure 5 (B) should not be interpreted as a molecular dissociation constant. In the molecular model, the time scale associated with the emergence of the apparent superdiffusive scaling is assigned to the time required for the molecules to escape the caging regime. This time scale is inversely proportional to the detachment rate, k_D, beyond which the stickers can detach and reattach to the network, moving the molecular center of mass in the process.[23] However, the length scale at which this caging regime is expected to occur is on the order of R_g (~ 10 nm for polymers in this work, Table S1), which is several orders of magnitude smaller than the experimentally accessible range of d^2 (0.5 – 52 μm) in this work. In the two-state model, k_{off} is interpreted as the phenomenological rate of conversion between the two apparent diffusing species postulated by the model. Thus, the decrease in k_{off} with concentration and sticker density in Figure 5(B) is consistent with the interpretation that an increased number of interchain bonds must be released to convert between the associated and the molecular states, as defined in the two-state model.

Since γK_{eq} is inversely proportional to the width of the superdiffusive regime, the increase in γK_{eq} with concentration and sticker density indicates that width of the apparent superdiffusive regime is decreasing with concentration and sticker density (Figure 5 (C)). This effect of concentration and sticker density is apparent when the self-diffusion data is plotted on non-dimensional axes using the fit parameters of the two-state model (Figure 6), such that the data is normalized by the transition from the late Fickian regime to the superdiffusive regime. In the two-

state model, the physical states of the two diffusion modes are not defined, and as such it is unable to predict the effect of increasing concentration. In the molecular model, the superdiffusive scaling occurs over a range of length scales where the molecules can hop faster than they can walk. Thus, superdiffusive scaling is hypothesized to be more apparent in associative networks where D_{hop} is significant. In the absence of intrachain bonds and assuming K_{eq} does not depend on *S*, the width of the apparent superdiffusive regime is expected to decrease with *S,* and eventually only Fickian scaling will be observed for *S*~5. When intrachain bonds are present, as is the case at low concentrations, the condition is relaxed further, and the superdiffusive scaling may be observed for chains with $S > 5$. For networks where superdiffusive scaling is observed, the model predicts that the width of the superdiffusive regime will decrease with increasing concentration, and this trend has been observed in earlier FRS measurements of unentangled networks [21-22] and is apparent in Figure 6 for all the polymers investigated in this work. This indicates that hopping becomes less prevalent for the gels at higher concentration due to the elimination of intrachain bonds. As for the effect of sticker density, Figure 5 (C) indicates that the width of the superdiffusive regime shows a very small decrease with sticker density for gels at 20% and 25% (w/v), which is consistent with the presence of more interchain bonds per chain with increasing *S*. For the gels at 15% (w/v), the width appears to increase with increasing sticker density, and this is due to the presence of a larger fraction of intrachain bonds for the PDHM15 gel compared to the PDHM10 gel at this concentration. While this qualitatively agrees with the predictions of the molecular model, the increase in γK_{eq} is significantly milder than predicted by the molecular model. This can be demonstrated by recasting the prediction of the molecular model in terms of the parameters in the two-state model. As demonstrated by Tang *et al.* the values of γK_{eq} can range between 0 and 1, where the limit of $\gamma K_{eq} = 1$ corresponds to pure Fickian scaling.[21] Thus, the prediction of the

molecular model can be recast in terms of the parameters in the two-state model as the following: γK_{eq} should increase with sticker density, such that above a critical value of *S*, where D_{hop} is not significant, γK_{eq} will approach the limiting value of 1, which corresponds to only Fickian diffusion. With $\gamma K_{eq} \approx 0.002$ for PDHM15 at 25% (w/v), this is several orders of magnitude smaller than the expected value of $\gamma K_{eq} = 1$. The limiting value of $\gamma K_{eq} = 1$ is shown as a black dashed line in Figure 6, and this shows that the width of the superdiffusive scaling regime spans at least two orders of magnitude, even for the PDHM15 gel at the highest concentration. From the earlier discussion of fitting the data to a single or sum of two exponential functions, it was demonstrated that $\langle \tau_2 \rangle$ for the PDHM15 gel at 25% (w/v) effectively captured the longest relaxation time (Figure 3(C)). Thus, it is clear that an extensive superdiffusive scaling regime is still observed even at the highest sticker density, and this result is unexpected since it implies that hopping remains an important mode of diffusion even for the polymer with $S = 15$.

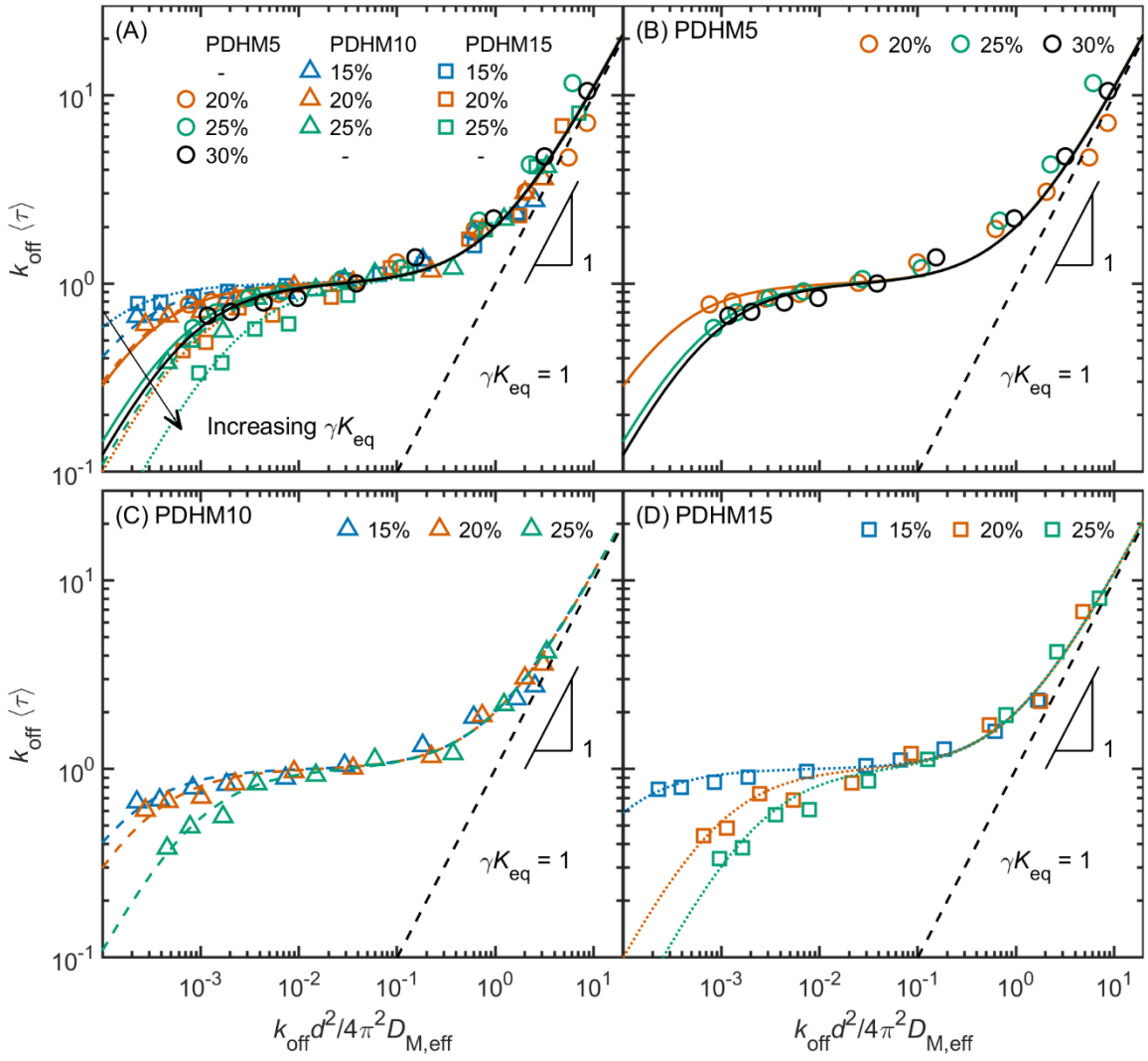

Figure 6. Diffusion data plotted in reduced parameter space. The dashed lines are fits to the two-state model. The black dashed line shows the case where $\gamma K_{eq} = 1$. Increasing the gel concentration and sticker density leads to a narrower range of d^2 spacing over which the apparent superdiffusive scaling is observed. The extent of the superdiffusive regime spans orders of magnitude even for the polymers with the highest sticker density.

Factors that promote hopping in high sticker-density polymers. The presence of intrachain bonds relaxes the condition for observing the apparent superdiffusive scaling in the theory, and the gels investigated in this work likely have a significant fraction of intrachain bonds. The fraction

of elastically active chains can be estimated from the viscosity, η of the gels as measured from frequency sweep experiments (Figure S4). The linear viscoelastic properties of polymers crosslinked with histidine-Ni^{2+} complexation have been investigated by other authors and the frequency sweep measurements show good agreement with the previously reported work, with relaxation times on the order of ~10 s.[11, 29-30] The sticky Rouse model predicts that η of the gel scales as $\eta \sim \phi^{5.9}$ for $\phi < \phi_s$ and $\eta \sim \phi^{1.1}$ for $\phi > \phi_s$.[20] The stronger scaling at lower concentrations emerges due to the conversion of intrachain bonds to interchain bonds. Above ϕ_s, most of the bonds are now interchain bonds, and the $\eta \sim \phi^{1.1}$ scaling emerges due to the higher density of crosslinks. While the gels investigated in this work are at concentrations that are above the calculated ϕ_s (**Table 2**), the strong scaling with concentration for η is more consistent with the regime $\phi < \phi_s$ (Figure 7). While it is difficult to obtain a quantitatively accurate estimate of the scaling exponent over a narrow region of concentration, it is suggestive of the presence of a significant fraction of intrachain bonds in the gels. This result is also consistent with the strong scaling seen with $D_{\mathrm{M,eff}}$ with concentration discussed earlier. This deviation from the prediction of the sticky Rouse model could be due to the assumptions applied in the model. This includes the assumption that the chains contain a large number of stickers per chain and have high degree of polymerization between the stickers, which may not hold for the polymers in this study.[20] Molecular dynamics simulation by Wang *et al.*[31] have shown that associative polymers with association strength of 1 – 10 k_BT can have a non-monotonic dependence of R_g with increasing S. As the sticker density is increased, the reduced spacing between the stickers results in the formation of higher fractions of intrachain bonds and this drives the collapse of the chains. The number fraction of elastically active strands estimated based on the affine network assumption was in the range of 0.8 – 1.0 for the highest concentration investigated for each polymer (Figure S5). Note

that the 20% uncertainty arises from the error associated with determining the monomer size.[32-33] This highlights the difficulty in accurately calculating the fraction of interchain and intrachain bonds from linear rheological properties. Additionally, in the development of the molecular model, it was predicted that above a critical concentration where the chains are strongly overlapping, only Fickian diffusion would be observed as hopping is no longer a dominant mode for diffusion. For the star polymers used in the molecular model, this critical concentration was predicted to be $\sim 10 \times \phi_S$, which is above the concentration for entanglement of those gels.[23] It is possible that the concentration where only Fickian diffusion would be observed for the gels in this study also lies above the entanglement concentration, a regime which was not investigated here.

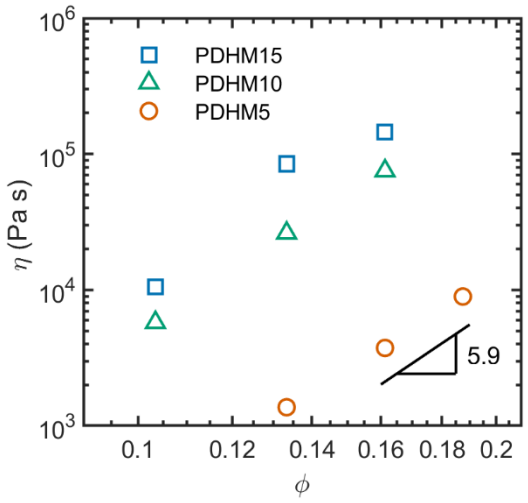

Figure 7. The zero-shear viscosity, η, as measured from frequency sweeps at 35 °C, as a function of the volume fraction of polymer, φ.

Also, the effective equilibrium binding constant K_{eff} has previously been suggested to decrease with sticker density due to the entropic penalty of having multiple stickers bound to the network.[24] Rapp *et al.* argued that with each additional sticker, the number of conformations the polymers can access is diminished further, and this can counteract the enthalpic penalty of stickers in the

dissociated state. Within this framework, the fraction of chains that have all their stickers in the dissociated state is predicted to be orders of magnitude higher than in the case where the effective equilibrium constant is assumed to be constant with respect to sticker density. For the case where K_{eff} is independent of *S*, the fraction of free chains [f] can be estimated from

$$[f]_S = \frac{1}{1 + K_{\mathrm{eff}}^S} \tag{8}$$

where $K_{\mathrm{eff}} = K_{\mathrm{eq}} \sim 300$ [25] such that $[f]_5 = 4.1 \times 10^{-13}$ and $[f]_{15} = 7.0 \times 10^{-38}$. For the case where K_{eff} decreases with *S*, [f] can be estimated from $D_{\mathrm{M,eff}}$, following the approach of Rapp *et al*. If the hopping diffusivity is dominant, then $D_{\mathrm{M,eff}} \sim D_{hop}$, where $D_{hop} = [f]D_0$ (D_0 is the diffusivity of a chain with no stickers). Thus $\frac{D_{M,eff,15}}{D_{M,eff,5}} = \frac{[f]_{15}}{[f]_5} = 0.104$ for the gels at 25% (w/v). Following the assumptions of Rapp *et al*., it appears that $\frac{[f]_{15}}{[f]_5}$ as estimated from $D_{\mathrm{M,eff}}$ is much larger than predicted if K_{eff} is independent of *S* (**Table 3**). This is qualitatively consistent with an entropic penalty for sticker association with the network. However, in the absence of an independent method to measure K_{eff}, it is difficult to test the validity of the assumptions made in this model.

Table 3. The ratio of the fraction of free stickers, $\frac{[f]_S}{[f]_5}$, as estimated from eq 8 and from the ratio of $D_{\mathrm{M,eff,S}}$.

	$S = 10$	$S = 15$
$\frac{1 + K_{\mathrm{eff}}^5}{1 + K_{\mathrm{eff}}^S} = \frac{[f]_S}{[f]_5}$	4.1×10^{-13}	1.7×10^{-25}
$\frac{D_{\mathrm{M,eff,S}}}{D_{\mathrm{M,eff,5}}} = \frac{[f]_S}{[f]_5}$	0.26 ± 0.01	0.02 ± 0.01

The presence of chains with lower sticker density can contribute to the observation of an apparent superdiffusive regime. The copolymers used in this work are expected to have a distribution of sticker densities that can be approximated with a Poisson distribution[34] (Figure 8). Note that the Poisson distribution is characterized by the property that the mean and variance are equal. Even with low dispersity ($Đ < 1.1$, Table S1), a substantial fraction of the chains in the highest sticker density PDHM15 gels can have sticker densities as low as 5 stickers per chain. As calculated previously from eq 8, the probability of releasing all its stickers to undergo hopping for a chain with 5 stickers is significantly higher than one with 15 stickers per chain. This effect may contribute to the observation of superdiffusive scaling for the PDHM15 gels. As demonstrated by Ramirez *et al*., the superdiffusive scaling is observed when two distinct diffusive modes result in the probability distribution of the center of mass for the dye-labelled species becoming non-Gaussian. Thus, for only Fickian scaling to be observed, the distribution must remain Gaussian for the entire range of length scales measured experimentally, which is only possible if there is no significant contribution to hopping, even from chains at the lowest end of the sticker density distribution.

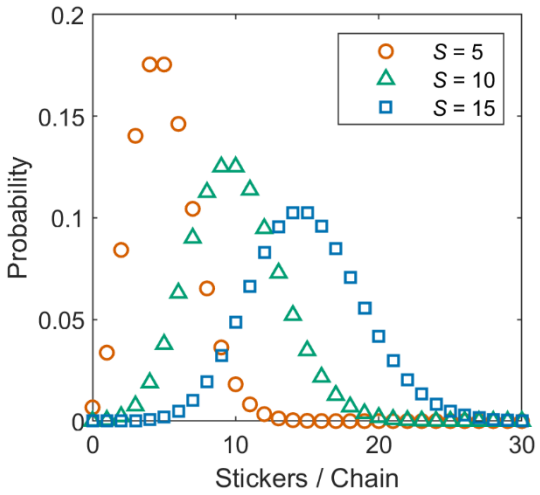

Figure 8. The probability distribution of sticker density for random copolymers is expected to follow a Poisson distribution[34], centered around the mean value of the sticker density, *S*.

Anomalous diffusion in polymers with fixed sticker spacing. While sticker spacing clearly affects the diffusivity of the polymers, it only has limited effect on the length scale over which the superdiffusive scaling is observed. This finding was demonstrated using a second set of polymers where the spacing between stickers *l* was kept constant and the number of stickers per chain *S* was varied from four to six by increasing the degree of polymerization *N* of the polymers. The value of *l* was chosen such that it corresponds to the *l* of PDHM5 (Figure 9). Note that polymers with sticker density higher than six for this set of polymers were not investigated since the molecular weight of the polymer would be above the molecular weight for entanglement at 25% (w/v). In contrast to the first set of polymers (PDHM5, PDHM10 and PDHM15), the concentration of stickers in the gel is constant with changing sticker number for this series of polymers.

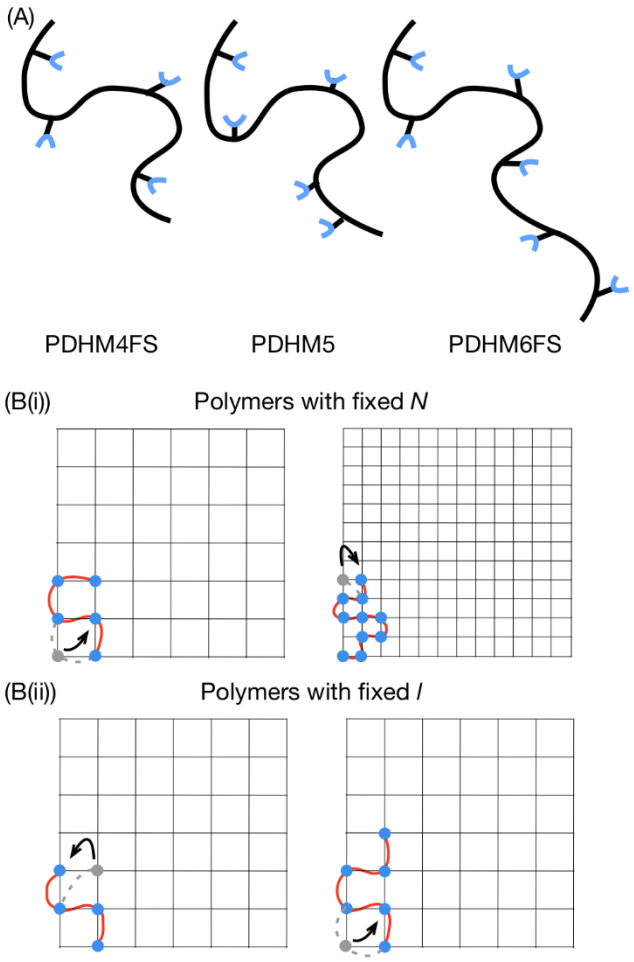

Figure 9. (A) The linear copolymers, of *N*,*N*-dimethyl-acrylamide and a histidine-functionalized monomer with fixed sticker spacing were synthesized by varying the ratio of EMP to the total monomer concentration to achieve average sticker densities, *S* of 4 and 6 stickers per chain. The sticker spacing, *l*~50, such that the degree of polymerization, $N=lS$ is different for each polymer. (B) The schematic shows the proposed walking distance for polymers with (i) fixed *N* and (ii) fixed *l*.

Similar to the trends seen with the polymers with fixed *N*, the diffusivity for the polymers with fixed spacing decreased with concentration and *S* as expected (Figure 10). The key difference for the polymers with fixed *N* is the observation that $D_{M,eff}$ and k_{off} for these polymers show a large

increase at lower concentrations with increasing *S*. This effect can be explained by considering the concentration for chain overlap, $\phi_{overlap}$ which decreases with *N*. As such, at a given concentration, PDHM6FS chains have greater overlap than PDHM4FS chains, leading to higher fractions of interchain bonds. Additionally, the $D_{\mathrm{M,eff}}$ of PDHM6FS, is comparable to PDHM10 for the gels at 25% (w/v) (Figure 5(A)). This is because this concentration is $\sim 4.5 \times \phi_s$ for PDHM6FS and $\sim 2.7 \times \phi_s$ for PDHM10 such that a larger fraction of the bonds in the PDHM6FS gels are interchain bonds. Similar to the polymers with fixed *N*, the width of the superdiffusive regime here showed a stronger dependence on concentration compared to the sticker density (Figure 11(C) and Figure 12). This indicates that the factors that promote hopping as discussed earlier are still important for these polymers (PDHM4FS, PDHM5 and PDHM6FS) and the modest effect of sticker density on the width of the superdiffusive regime (Figure 6) was not just an effect of the different spacing between the stickers.

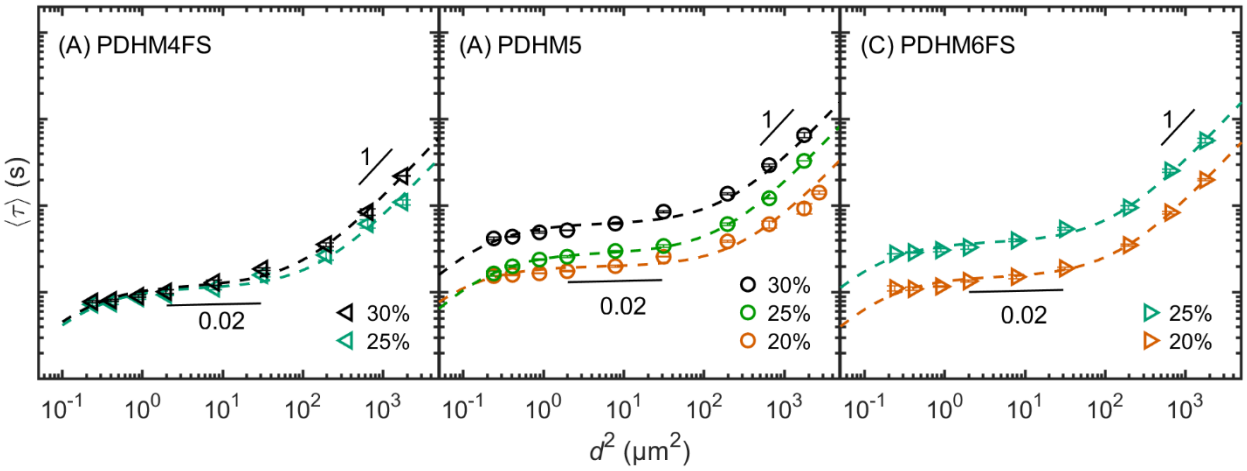

Figure 10. Plot of $\langle\tau\rangle$ vs d^2 for (A) PDHM4FS, (B) PDHM5 and (C) PDHM6FS at 20%, 25% and 30% (w/v), measured at 35 °C. The sticker spacing was held constant, while the sticker density was increased. The dashed lines are fits to the two-state model. Error bars represent standard error of measurements performed in triplicate.

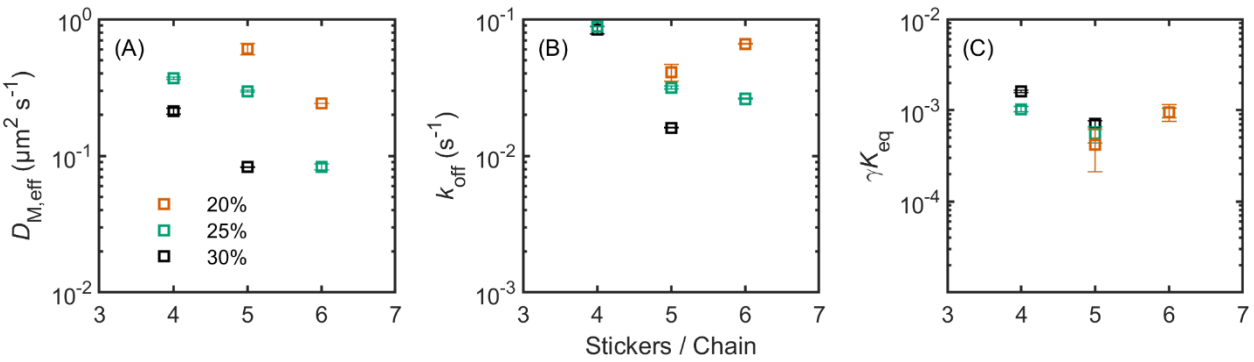

Figure 11. Effect of sticker density on (A) the effective diffusivity in the large-length-scale Fickian regime, $D_{M,eff}$ (B) the molecular dissociation rate, k_{off} and (C) γK_{eq}. The parameters were obtained by fitting the analytical solution of the two-state model to the experimentally derived relation $\langle\tau\rangle$ vs d^2 for gels at various concentrations. Error bars represent 95% confidence intervals from fits to the two-state model.

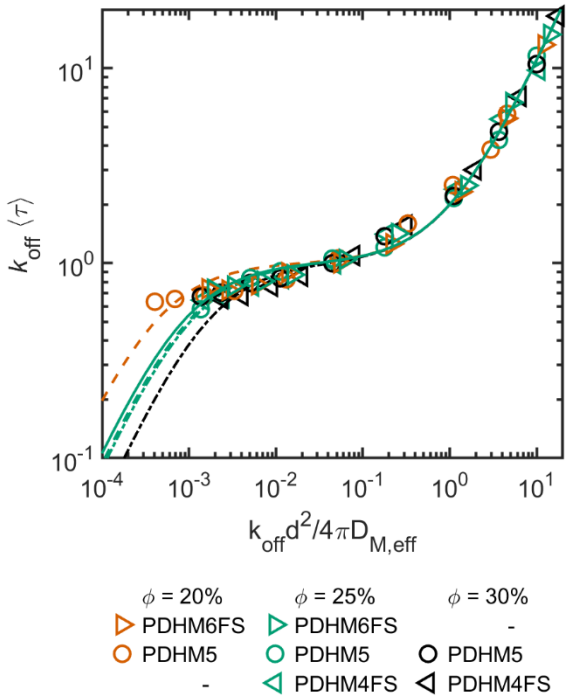

Figure 12. Diffusion data for polymers with fixed l plotted in reduced parameter space. The dashed lines are fits to the two-state model.

CONCLUSION

Using a set of linear side-functionalized polymers with sticker densities up to 15 stickers per chain, this work characterized self-diffusion within gels in the unentangled regime. An apparent superdiffusive regime was observed for all the gels studied which suggests that hopping is a significant mode of diffusion, even for the polymer with 15 stickers per chain. Despite the presence of two relaxation modes, corresponding to the two diffusive modes as predicted by earlier models, it was shown that single exponential fits offered a reasonable approximation and provided consistent fit results to the intensity decay data obtained from experiments. From fits of the diffusion data to the earlier two-state model, the model parameters were extracted. The diffusivity within the large Fickian regime decreased with concentration and sticker density as predicted by the mean-field sticky Rouse model. However, the scaling of the diffusivity with increasing concentration was stronger than expected. This suggests a presence of significant fractions of intrachain bonds even though the concentrations investigated were above the concentration for overlap of the strand between stickers, a regime wherein the fraction of intrachain bonds should be negligible. The width of the superdiffusive regime decreased with concentration and to a lesser extent, with sticker density. In fact, the superdiffusive regime was still well-developed even for the polymer with 15 stickers per chain which was not expected based on the predictions of the molecular model.

Further investigation of the viscoelastic properties of the gels showed that the conversion of intrachain to interchain bonds is likely responsible for the decrease in the width of the superdiffusive regime with increasing concentration. Additionally, the strong scaling of viscosity

with concentration provides further evidence of a significant fraction of intrachain bonds, consistent with the observation of strong concentration dependence of the diffusivity. The strong presence of intrachain bonds could help explain the modest effect of sticker density on the range over which the apparent superdiffusive scaling is observed. While the sticky Rouse model predicts that the fraction of intrachain bonds should be negligible for gels that were prepared at concentrations above those for overlap of the strand between stickers, the scaling presented by the model did not take into account that the formation of intrachain bonds can cause the collapse of the chains. Such chain collapse could result in an expansion of the concentration regime dominated by the presence of intrachain bonds. Other factors not considered in the previously proposed molecular model for diffusion can contribute to the results reported here. These factors include the role of entropic penalty in reducing the effective equilibrium constant and the distribution of sticker densities inherent to polymers synthesized by RAFT copolymerization. Additional experiments with polymers where the spacing between the stickers are kept constant as the sticker density is increased also showed minimal effect of sticker density on the width of the superdiffusive regime, thereby indicating that the factors that promote hopping were not solely dependent on the spacing between stickers.

ASSOCIATED CONTENT

The Supporting Information is available at [link inserted by publisher]

Supplementary figures, tables and discussion on pH of gels, error estimation for fits using one or sum of two exponential functions and scaling diffusivity from sticky Rouse model.

AUTHOR INFORMATION

Corresponding Author

*(N.H-A) Email holten@mit.edu

*(B.D.O) Email bdolsen@mit.edu

Notes

The authors declare no competing financial interest.

ACKNOWLEDGMENT

This work was supported in part by the MRSEC Program of the National Science Foundation under award number DMR - 1419807, the National Science Foundation under Award DMR-1709315, the U.S. Army Research Office through the Institute for Soldier Nanotechnologies under Contract W911NF-07-D-0004 and the Office of Naval Research (ONR) under the Young Investigators Program Grant ONR.N00014-15-1-2763. The authors thank G. Wei for help with refinement of the polymer purification method.

REFERENCES

1. Li, C. H.; Wang, C.; Keplinger, C.; Zuo, J. L.; Jin, L.; Sun, Y.; Zheng, P.; Cao, Y.; Lissel, F.; Linder, C.; You, X. Z.; Bao, Z., A highly stretchable autonomous self-healing elastomer. *Nat Chem* **2016,** *8* (6), 618-24.
2. Tee, B. C.; Wang, C.; Allen, R.; Bao, Z., An electrically and mechanically self-healing composite with pressure-and flexion-sensitive properties for electronic skin applications. *Nature nanotechnology* **2012,** *7* (12), 825.
3. Sanoja, G. E.; Schauser, N. S.; Bartels, J. M.; Evans, C. M.; Helgeson, M. E.; Seshadri, R.; Segalman, R. A., Ion Transport in Dynamic Polymer Networks Based on Metal–Ligand Coordination: Effect of Cross-Linker Concentration. *Macromolecules* **2018,** *51* (5), 2017-2026.

4. Zhang, Q.; Niu, S.; Wang, L.; Lopez, J.; Chen, S.; Cai, Y.; Du, R.; Liu, Y.; Lai, J. C.; Liu, L., An Elastic Autonomous Self-Healing Capacitive Sensor Based on a Dynamic Dual Crosslinked Chemical System. *Advanced Materials* **2018,** *30* (33), 1801435.
5. Bode, S.; Zedler, L.; Schacher, F. H.; Dietzek, B.; Schmitt, M.; Popp, J.; Hager, M. D.; Schubert, U. S., Self-healing polymer coatings based on crosslinked metallosupramolecular copolymers. *Advanced Materials* **2013,** *25* (11), 1634-1638.
6. Scheltjens, G.; Diaz, M.; Brancart, J.; Van Assche, G.; Van Mele, B., A self-healing polymer network based on reversible covalent bonding. *Reactive and Functional Polymers* **2013,** *73* (2), 413-420.
7. Glassman, M. J.; Olsen, B. D., Structure and mechanical response of protein hydrogels reinforced by block copolymer self-assembly. *Soft matter* **2013,** *9* (29), 6814-6823.
8. Guvendiren, M.; Lu, H. D.; Burdick, J. A., Shear-thinning hydrogels for biomedical applications. *Soft matter* **2012,** *8* (2), 260-272.
9. Wever, D.; Picchioni, F.; Broekhuis, A., Polymers for enhanced oil recovery: a paradigm for structure–property relationship in aqueous solution. *Progress in Polymer Science* **2011,** *36* (11), 1558-1628.
10. Taylor, K. C.; Nasr-El-Din, H. A., Water-soluble hydrophobically associating polymers for improved oil recovery: A literature review. *Journal of Petroleum Science and Engineering* **1998,** *19* (3-4), 265-280.
11. Grindy, S. C.; Lenz, M.; Holten-Andersen, N., Engineering elasticity and relaxation time in metal-coordinate cross-linked hydrogels. *Macromolecules* **2016,** *49* (21), 8306-8312.
12. Rossow, T.; Seiffert, S., Supramolecular polymer gels with potential model-network structure. *Polymer Chemistry* **2014,** *5* (8), 3018.
13. Brassinne, J.; Jochum, F. D.; Fustin, C. A.; Gohy, J. F., Revealing the supramolecular nature of side-chain terpyridine-functionalized polymer networks. *Int J Mol Sci* **2015,** *16* (1), 990-1007.
14. Wang, R.; Geven, M.; Dijkstra, P. J.; Martens, P.; Karperien, M., Hydrogels by supramolecular crosslinking of terpyridine end group functionalized 8-arm poly(ethylene glycol). *Soft Matter* **2014,** *10* (37), 7328-36.
15. Yang, Y. J.; Mai, D. J.; Dursch, T. J.; Olsen, B. D., Nucleopore-Inspired Polymer Hydrogels for Selective Biomolecular Transport. *Biomacromolecules* **2018,** *19* (10), 3905-3916.
16. Maguire, L.; Stefferson, M.; Betterton, M. D.; Hough, L. E., Design principles of selective transport through biopolymer barriers. *Phys Rev E* **2019,** *100* (4-1), 042414.
17. Stukalin, E. B.; Cai, L. H.; Kumar, N. A.; Leibler, L.; Rubinstein, M., Self-Healing of Unentangled Polymer Networks with Reversible Bonds. *Macromolecules* **2013,** *46* (18).
18. Olsen, B. D.; Kornfield, J. A.; Tirrell, D. A., Yielding behavior in injectable hydrogels from telechelic proteins. *Macromolecules* **2010,** *43* (21), 9094-9099.
19. Baxandall, L.; Edwards, S., Deformation-dependent properties of polymer networks constructed by addition of crosslinks under strain. *Macromolecules* **1988,** *21* (6), 1763-1772.
20. Rubinstein, M.; Semenov, A. N., Dynamics of entangled solutions of associating polymers. *Macromolecules* **2001,** *34* (4), 1058-1068.
21. Tang, S.; Wang, M.; Olsen, B. D., Anomalous self-diffusion and sticky Rouse dynamics in associative protein hydrogels. *J Am Chem Soc* **2015,** *137* (11), 3946-57.
22. Tang, S.; Habicht, A.; Li, S.; Seiffert, S.; Olsen, B. D., Self-Diffusion of Associating Star-Shaped Polymers. *Macromolecules* **2016,** *49* (15), 5599-5608.

23. Ramirez, J.; Dursch, T. J.; Olsen, B. D., A Molecular Explanation for Anomalous Diffusion in Supramolecular Polymer Networks. *Macromolecules* **2018,** *51* (7), 2517-2525.
24. Rapp, P. B.; Omar, A. K.; Silverman, B. R.; Wang, Z. G.; Tirrell, D. A., Mechanisms of Diffusion in Associative Polymer Networks: Evidence for Chain Hopping. *J Am Chem Soc* **2018,** *140* (43), 14185-14194.
25. Tang, S.; Olsen, B. D., Relaxation Processes in Supramolecular Metallogels Based on Histidine-Nickel Coordination Bonds. *Macromolecules* **2016,** *49* (23), 9163-9175.
26. Wang, M.; Timachova, K.; Olsen, B. D., Diffusion Mechanisms of Entangled Rod-Coil Diblock Copolymers. *Macromolecules* **2013,** *46* (14), 5694-5701.
27. Wang, M.; Timachova, K.; Olsen, B. D., Experimental Measurement of Coil-Rod-Coil Block Copolymer Tracer Diffusion through Entangled Coil Homopolymers. *Macromolecules* **2013,** *46* (4), 1651-1658.
28. Hackelbusch, S.; Rossow, T.; van Assenbergh, P.; Seiffert, S., Chain Dynamics in Supramolecular Polymer Networks. *Macromolecules* **2013,** *46* (15), 6273-6286.
29. Fullenkamp, D. E.; He, L.; Barrett, D. G.; Burghardt, W. R.; Messersmith, P. B., Mussel-inspired histidine-based transient network metal coordination hydrogels. *Macromolecules* **2013,** *46* (3), 1167-1174.
30. Grindy, S. C.; Learsch, R.; Mozhdehi, D.; Cheng, J.; Barrett, D. G.; Guan, Z. B.; Messersmith, P. B.; Holten-Andersen, N., Control of hierarchical polymer mechanics with bioinspired metal-coordination dynamics. *Nature Materials* **2015,** *14* (12), 1210-1216.
31. Carrillo, J.-M. Y.; Chen, W.-R.; Wang, Z.; Sumpter, B. G.; Wang, Y., Chain conformation of polymer melts with associating groups. *Journal of Physics Communications* **2019,** *3* (3), 035007.
32. Zhang, X.; Liu, C.; Wang, Z., Force spectroscopy of polymers: Studying on intramolecular and intermolecular interactions in single molecular level. *Polymer* **2008,** *49* (16), 3353-3361.
33. Wang, C.; Shi, W.; Zhang, W.; Zhang, X.; Katsumoto, Y.; Ozaki, Y., Force spectroscopy study on poly (acrylamide) derivatives: Effects of substitutes and buffers on single-chain elasticity. *Nano Letters* **2002,** *2* (10), 1169-1172.
34. Stockmayer, W. H., Distribution of Chain Lengths and Compositions in Copolymers. *The Journal of Chemical Physics* **1945,** *13* (6), 199-207.

For Table of Contents use only

Anomalous Diffusion in Associative Networks of High Sticker-density Polymers

Irina Mahmad Rasid,[†] *Niels Holten-Andersen*[*,†] *and Bradley D. Olsen*[*,‡]

[†] Department of Materials Science and Engineering, Massachusetts Institute of Technology, 77 Massachusetts Avenue, Cambridge, Massachusetts 02139, United States

[‡] Department of Chemical Engineering, Massachusetts Institute of Technology, 77 Massachusetts Avenue, Cambridge, Massachusetts 02139, United States